Probing calculated O_{2}^{+} potential-energy curves with an XUV-IR pump-probe experiment

Philipp Cörlin, Andreas Fischer, Michael Schönwald, Alexander Sperl, Tomoya Mizuno, Uwe Thumm, Thomas Pfeifer, and Robert Moshammer

Phys. Rev. A **91**, 043415 — Published 22 April 2015

DOI: 10.1103/PhysRevA.91.043415

Probing calculated O_2^+ potential-energy curves with an XUV–IR pump–probe experiment

Philipp Cörlin,[1,*] Andreas Fischer,[1] Michael Schönwald,[1] Alexander Sperl,[1]
Tomoya Mizuno,[1] Uwe Thumm,[2] Thomas Pfeifer,[1] and Robert Moshammer[1,†]

[1] *Max-Planck-Institut für Kernphysik, Saupfercheckweg 1, 69117 Heidelberg, Germany*
[2] *J. R. Macdonald Laboratory, Department of Physics,*
Kansas State University, Manhattan, Kansas 66506, USA

We study dissociative photo-ionization of molecular oxygen in a kinematically complete XUV–IR pump–probe experiment. Detecting charged fragments and photoelectrons in coincidence using a reaction microscope, we observe a pump–probe delay-dependent yield of very low energetic O^+ ions which oscillates with a period of 40 fs. This feature is caused by a time-dependent vibrational wave packet in the potential of the binding $O_2^+(a\,^4\Pi_u)$ state, which is probed by resonant absorption of a single infrared photon to the weakly repulsive $O_2^+(f\,^4\Pi_g)$ state. By quantitative comparison of the experimental kinetic-energy-release (KER) and quantum-beat (QB) spectra with the results of a coupled-channel simulation, we are able to discriminate between the calculated adiabatic O_2^+ potential-energy curves (PECs) of Marian et al., Mol. Phys. **46**, 779 (1982) and Magrakvelidze et al., Phys. Rev. A **86**, 023402 (2012). In general, we find a good agreement between experimental and simulated KER and QB spectra. However, we could not reproduce all features of the experimental data with these PECs. In contrast, adjusting a Morse potential to the experimental data, most features of the experimental spectra are well reproduced by our simulation. By comparing this Morse potential to theoretically predicted PECs, we demonstrate the sensitivity of our experimental method to small changes in the shape of the binding potential.

PACS numbers: 33.80.Wz, 33.20.Tp, 33.15.Mt

I. INTRODUCTION

The ionization of molecules leads to the coherent excitation of a multitude of vibrational states often belonging to various ionic potential-energy curves (PECs). Due to their different eigenenergies, these vibrational states exhibit different phase evolutions and their superposition leads to a time-dependent nuclear vibrational wave packet. Its time evolution is determined by the vibrational level spacing which is in the order of 100 meV for light diatomic molecules. This translates into typical oscillation periods of a few tens of femtoseconds. In order to temporally resolve the evolution of such a wave packet, laser pulses shorter than the oscillation period have to be employed.

For H_2, the simplest neutral molecule, vibrational wave packets have been extensively studied exploring pump–probe techniques throughout the last decade [1–5]. While only a single binding electronic state exists in H_2^+, more complex diatomic molecules feature a large variety of bound ionic states (a selection of PECs of O_2^+ is plotted in Fig. 1). This complicates the interpretation of experimental KER spectra and might explain why the detailed wave-packet dynamics in atmospherically relevant diatomic molecules such as N_2 or O_2 [6–9] has been investigated less frequently than in H_2^+ and its isotopes.

A few years ago the nuclear vibrational motion in a binding O_2^+ molecular state was observed in an IR–IR (infrared) pump–probe experiment [7]. Soon after that quantum simulations [8] confirmed the interpretation that in this experiment strong-field ionization to the binding $O_2^+(a\,^4\Pi_u)$ state by an intense laser pulse launches a molecular wave packet. This state can be coupled to the weakly repulsive $O_2^+(f\,^4\Pi_g)$ state by an IR probe pulse which causes the molecule to dissociate (Fig. 2). In these experiments very intense laser pulses (up to $3 \times 10^{14}\,\mathrm{W/cm^2}$) were used which cannot be treated perturbatively. The general agreement between theory and experiment is good. However, discrepancies remain between the measured and simulated quantum-beat frequencies. Furthermore, measured O^+ kinetic-energy release (KER) spectra show distinct maxima in the O^+ yield which are not reproduced in simulated spectra.

In our XUV–IR pump–probe experiment, we use an extreme ultraviolet (XUV) pulse to initiate the wave-packet oscillation by single-photon ionization and probe the dynamics with a weak IR pulse ($\approx 3 \times 10^{12}\,\mathrm{W/cm^2}$). Therefore perturbation of the PECs during the pump and probe step is small. Compared to strong-field experiments with intense IR pulses [7], this is advantageous as our goal here is the investigation of the unperturbed, field-free molecular dynamics on specific PECs. An XUV–XUV pump–probe technique would be the method of choice to perform such an experiment since the interaction of the excited molecular cation with the probe pulse would be weaker. In state-of-the-art experiments with XUV pulses, however, pulse durations were too long to allow a temporal resolution of the wave-packet dynamics in O_2^+ [11].

---

[*] philipp.coerlin@mpi-hd.mpg.de
[†] robert.moshammer@mpi-hd.mpg.de

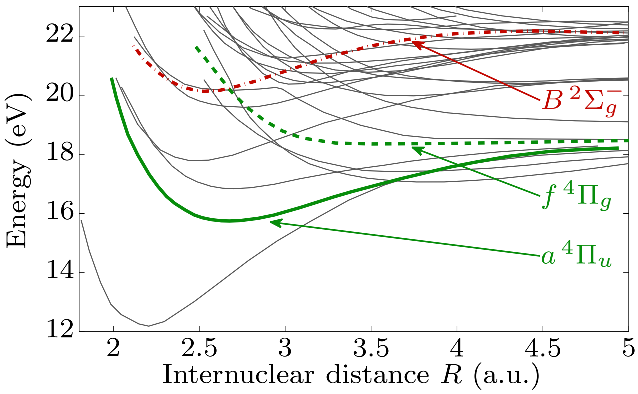

Figure 1. (Color online) Selection of O_2^+ PECs from Ref. [10]. We consider i) a vibrational wave packet that oscillates within the $O_2^+(a\,^4\Pi_u)$ potential (bold green solid curve) and is probed to the $O_2^+(f\,^4\Pi_g)$ PEC (bold green dashed curve) and ii) predissociation out of the $O_2^+(B\,^2\Sigma_g^-)$ state (bold red dash-dotted curve).

Within the framework of a coupled-channel simulation we show that the wave-packet dynamics is very sensitive to the shape of the binding potential and that the kinetic energies of measured O^+ fragments strongly depend on the PEC associated with the final anti-bonding adiabatic state of the molecular cation. This enables us to discriminate between different calculated PECs. Quantum-mechanical simulations performed using a Morse potential adjusted to the experimental data provide additional scrutiny of the accurate shape of the involved binding PEC.

II. EXPERIMENTAL SETUP

In our experiment 30(5) fs IR laser pulses at a repetition rate of 8 kHz are spectrally broadened within a neon-filled hollow-core fiber and re-compressed using chirped mirrors. We achieve a pulse duration of approximately 12(3) fs at a center wavelength of 760 nm. The pulses are divided in a pump and a probe pulse by a beam splitter (Fig. 3) within a vacuum chamber.

In the first beam path an attosecond pulse train is created via high-harmonic generation (HHG) within an argon-filled gas cell (labeled ‘HHG target’ in Fig. 3) [12]. Behind an aluminum filter (labeled ‘Al filter’ in Fig. 3), which blocks the copropagating fundamental light, the created XUV radiation in the energy range between 17 and 40 eV is focused by a pair of mirrors (labeled ‘focusing mirrors’ in Fig. 3) into a reaction microscope [13].

Within the second beam path a retro reflector (Fig. 3) on a motorized delay stage is used to vary the optical path length of the IR probe pulse. This allows us to introduce large pump–probe delays of up to 10 ps. The intensity of the probe pulse is controlled by a motorized iris aperture (Fig. 3).

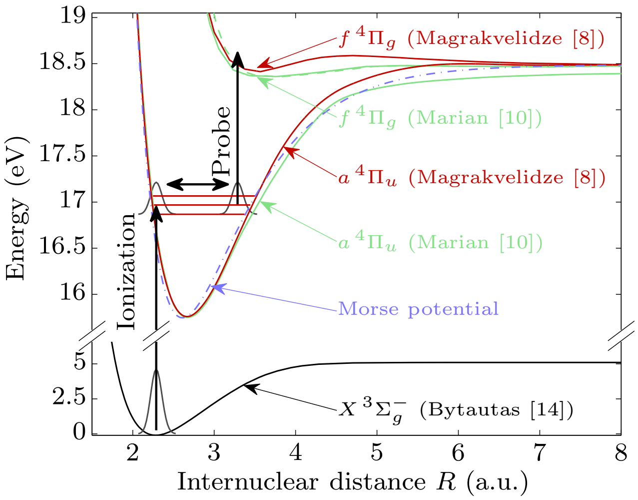

Figure 2. (Color online) Relevant O_2^+ PECs. The neutral O_2 ground-state potential (black curve) is taken from Ref. [14]. A Morse potential (blue dash-dotted curve) has been adjusted to our experimentally observed quantum-beat frequency and revival time. Relevant vibrational states within this potential are plotted as red horizontal lines. The potentials of the binding $a\,^4\Pi_u$ state are taken from Refs. [8] (red [dark gray] curve) and [10] (green [light gray] curve). Absorption of a single IR photon transfers population to the repulsive $O_2^+(f\,^4\Pi_g)$ state taken from Refs. [8] (red [dark gray] curve) and [10] (green [light gray] curve). The dashed green curve is the latter curve shifted by 0.08 a.u. towards larger internuclear distances.

Both beams are collinearly overlapped behind a parabolic mirror (Fig. 3), with a hole drilled along the cylinder axis. The XUV pulses are guided through this hole while the parabolic mirror focuses the IR pulse into the reaction volume of the reaction microscope. We reach effective IR intensities of $3 \times 10^{12}\,\mathrm{W/cm^2}$ within the pulse overlap.

In the center of the reaction microscope a gas jet (Fig. 3) of O_2 molecules intersects the laser foci. Created photoions and photoelectrons are guided towards position-sensitive micro-channel-plate detectors (labeled ‘MCP’ in Fig. 3) using electric and magnetic fields. The initial three-dimensional momenta of all charged particles can be reconstructed from the particles’ measured flight times and hit positions on the detector. This allows us to obtain kinematically complete information with full solid-angle acceptance.

III. EXPERIMENTAL RESULTS

The main observable is a pump–probe time-delay-dependent yield of low-energetic O^+ fragments [Fig. 4 (a)]. For this we consider the reaction

$$O_2 \xrightarrow{\mathrm{XUV}} O_2^+(a^4\,\Pi_u) + e^- \xrightarrow{\mathrm{IR}} (O^+ + O)(f\,^4\Pi_g) + e^- .$$

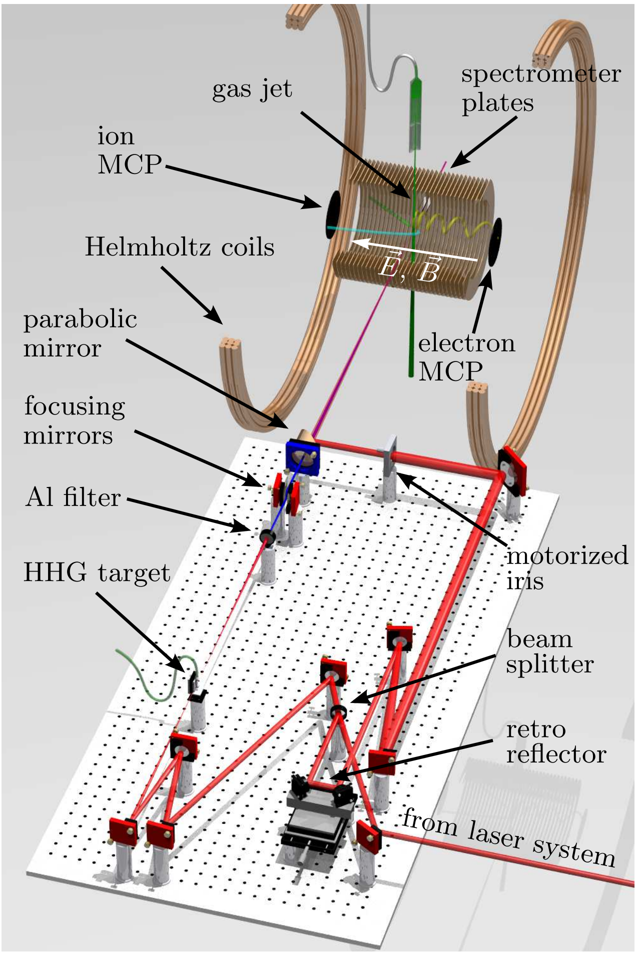

Figure 3. Schematic of the reaction microscope and the interferometer for the generation of mutually delayed XUV pump and IR probe pulses, including: Micro-channel-plate detector (MCP), aluminum filter (Al filter), high-harmonic-generation target (HHG target). The parallel homogeneous electric and magnetic fields within the spectrometer are represented by the white arrow.

In the pump step, neutral oxygen molecules are ionized to the binding $O_2^+(a\,^4\Pi_u)$ electronic state (Fig. 2). Due to the coherent excitation of multiple vibrational states, a molecular wave packet is launched and oscillates within the corresponding PEC. The probe pulse couples the two states around an internuclear distance of $R_c \approx 3.2\,\text{a.u.}$ (Fig. 2). The population transfered to the repulsive $O_2^+(f\,^4\Pi_g)$ state depends on the pump–probe delay, resulting in the observed time-delay-dependent yield of O^+ fragments. Since the $f\,^4\Pi_g$ PEC is flat for $R \gtrsim R_c$, these fragments exhibit a low KER.

A. Wave-packet oscillation in the time domain

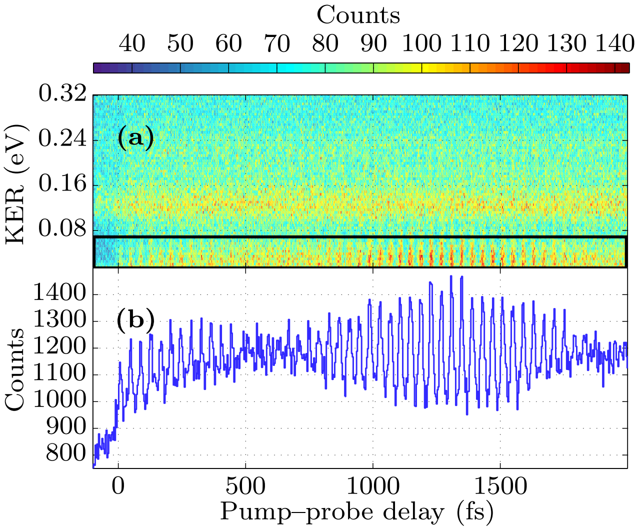

Figure 4. **(a)** Number of detected O^+ fragments as a function of pump–probe delay and KER. **(b)** Projection of events within the black box in (a) onto the time-delay axis. For positive delays, the XUV pulse precedes the IR pulse.

The experimentally observed O^+ counts are shown in Fig. 4 (a) as a function of the pump–probe delay and the $\text{KER} = E_{\text{kin}}^{\text{O}^+} + E_{\text{kin}}^{\text{O}} \approx 2E_{\text{kin}}^{\text{O}^+}$. For $\text{KER} < 0.08\,\text{eV}$ an oscillatory behavior of the yield with a period of 40 fs is clearly visible. The projection of the events indicated by the black box in Fig. 4 (a) onto the time-delay axis is shown in Fig. 4 (b).

The oscillation amplitude [Fig. 4 (b)] varies as a function of the time delay. This is caused by the anharmonicity of the $a\,^4\Pi_u$ PEC: as the spacings of the vibrational energies are not equidistant, the originally well localized wave packet dephases over a period of approximately 640 fs before it revives after 1270 fs. Surprisingly the oscillation amplitude within the revival structure is much larger than close to the temporal overlap of pump and probe pulse. This is in contrast to previous experiments on H_2 where the modulation within the revivals at increasingly larger time-delay was observed to be decreasing [15].

A possible explanation for this interesting feature in our data might be an increased ionization cross section to the $a\,^4\Pi_u$ state for perpendicular orientation between molecular axis and XUV polarization. For photon energies between 30 and 40 eV, where our XUV spectrum is most intense, this assumption is supported by quantum mechanical calculations in Ref. [16]. Since the resonant probing process is only allowed for parallel transitions, i.e., for molecules oriented along the IR-pulse polarization direction, (Fig. 5 (b) and subsection III C), the molecular ion might require some time to align correctly to the probe field. This is further plausible since typical rotational periods of O_2 are (depending on the excited rotational states) of the order of hundreds of femtoseconds to a few picoseconds.

The time independent signal in Fig. 4 at $\text{KER} \approx 0.12\,\text{eV}$ most likely originates from ioniza-

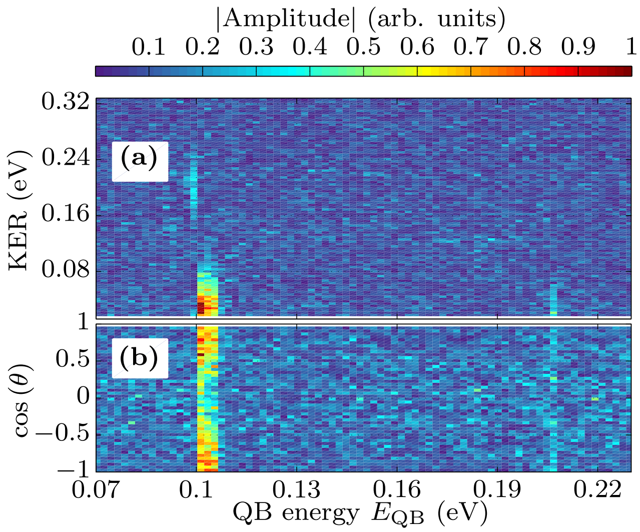

Figure 5. **(a)** QB spectrum of the data shown in Fig. 4 (a). The distinct lines in the QB energy result from the oscillatory behavior of the O^+ yield as a function of the time delay. **(b)** Amplitude of the Fourier transform of the delay-dependent yield of low energetic O^+ ions as a function of $\cos(\theta)$. The angle θ designates the orientation of the molecular axis relative to the identical linear polarization directions of the XUV and IR pulses.

tion to the $\mathrm{O}_2^+(B\,^2\Sigma_g^-)$ state (red line in Fig. 1) that predissociates to the $\mathrm{O}(^1\mathrm{D}) + \mathrm{O}^+(^4\mathrm{S}^0)$ continuum for $v \geq 4$, resulting in O^+ fragments at the observed energy. This predissociation channel was reported in a previous measurement [17]. Experimental data for KER $< 0.013\,\mathrm{eV}$ is not plotted in Fig. 4 as for these energies a background of stable O_2^{2+} (which has the same time-of-flight as very low energetic O^+ ions) dominates.

B. Wave-packet oscillation in the frequency domain

For a quantitative analysis of the beat frequencies we perform a Fourier transform at fixed KERs over the interval $[0, 2\,\mathrm{ps}]$ of the delay scan in Fig. 4 (a). In Fig. 5 (a) the absolute value of the obtained Fourier amplitude is plotted as a function of the KER and the quantum-beat (QB) energy, which is defined as $E_{\mathrm{QB}} = \hbar\omega_{\mathrm{QB}}$. Here the QB frequency ω_{QB} is the Fourier complementary variable of the pump–probe delay.

The strongest line at low KER and $E_{\mathrm{QB}} \approx 0.104\,\mathrm{eV}$ corresponds to the visible oscillation in the time domain that is created by the beating between neighboring vibrational states. The QB energy coincides with the expected vibrational level spacings $E_{v=10} - E_{v=9} = 0.103\,\mathrm{eV}$ and $E_{v=9} - E_{v=8} = 0.106\,\mathrm{eV}$ of the $a\,^4\Pi_u$ state calculated in Ref. [8]. In the experimental data these two energies are not resolved because the time-delay range of 2 ps is too short to allow their separation in the frequency domain.

An additional weak signal at KER $\approx 0.22\,\mathrm{eV}$ originates from the beating of higher lying vibrational states (most likely $v = 11$ and $v = 10$). Due to the anharmonicity of the binding potential this beating occurs at slightly lower QB energies than the beating between the states with $v = 8$, 9, and 10. A third weak signal at $E_{\mathrm{QB}} \approx 0.207\,\mathrm{eV}$ is caused by the beating between vibrational states with $\triangle v = 2$ (most likely $v = 10$ and $v = 8$).

C. Identification of potential-energy curves

Next, we show that the involved ionic PECs are corresponding to the binding $\mathrm{O}_2^+(a\,^4\Pi_u)$ state and the repulsive $\mathrm{O}_2^+(f\,^4\Pi_g)$ state. We will describe several features which allow us to identify adiabatic PECs on which the nuclear motion occurs from the experimental data. A quantity important for the identification of the PECs is the angular dependence of the oscillatory signal. A Fourier transform of the low energetic O^+ yield as a function of the time delay and $\cos(\theta)$ is shown in Fig. 5 (b). Here θ denotes the angle between the IR polarization and molecular axis. Experimentally, the alignment of the molecule is reconstructed from the momentum vector of the O^+ ion. The values $\cos(\theta) = \pm 1$ correspond to molecules aligned along and $\cos(\theta) = 0$ perpendicular to the laser polarization.

Figure 5 (b) shows that the oscillation is strongest for parallel alignment where the coupling between the binding and the anti-binding PEC is strongest. Applying dipole selection rules, this observation significantly reduces the number of possible PECs.

Two additional selection criteria for relevant PECs are given by the very low KERs and the measured QB energies. The former demand a flat repulsive potential and the latter must agree with calculated vibrational energy spacings of the binding PEC (see Fig. 5 (a) and Fig. 4). To our best knowledge, these three conditions are only fulfilled by the binding $a\,^4\Pi_u$ and the repulsive $f\,^4\Pi_g$ electronic state of O_2^+. The large photo-ionization cross-section to the $^4\Pi_u$ state measured in Refs. [18, 19] and calculated in Ref. [16] points to this intermediate state as well. Last but not least, the very good agreement between the experimental spectra and the results from coupled-channel simulations shown in the next section further support our hypothesis.

IV. THEORETICAL DESCRIPTION

To gain a deeper understanding of the experimental data we perform coupled-channel simulations with different sets of PECs (for the used method see Ref. [7, 8, 11, 20]).We apply the Franck-Condon approximation and assume that the vibrational ground-state of the potential belonging to the neutral $X\,^3\Sigma_g^-$ state (taken from Ref. [14]) is vertically promoted to the binding $\mathrm{O}_2^+(a\,^4\Pi_u)$ PEC. In this potential the vibrational wave packet is propagated and coupled by the probe laser pulse to the $O_2^+(f\,^4\Pi_g)$ state.

In the following we present the results of our simulation for three different pairs of binding and repulsive PECs and compare them to experiment. This allows us to test the predicted shapes of the involved PECs. In subsection IV A the wave packet is propagated in the binding potential calculated by Magrakvelidze et al. [8] (red [dark gray] curve in Fig. 2). Next, in subsection IV B, we simulate the wave-packet dynamics in the binding $O_2^+(a\,^4\Pi_u)$ PEC theoretically predicted by Marian et al. [10] (green [light gray] curve in Fig. 2). Since the simulated QB energy and revival time based on the $O_2^+(a\,^4\Pi_u)$ from Refs. [7, 8] show some discrepancy with the experimental spectra, we also propagate the wave packet within a Morse potential (blue dash-dotted curve in Fig. 2) adjusted to our experimental data as discussed in subsection IV C.

In all three cases the binding $a\,^4\Pi_u$ state is coupled to the repulsive $f\,^4\Pi_g$ state calculated by Ref. [10] (green [light gray] curve in Fig. 2), and the simulated yield of O^+ fragments as a function of the pump–probe time delay and KER is compared to the experimental spectra. If the wave-packet is instead coupled to the repulsive $f\,^4\Pi_g$ state calculated by Ref. [8] (red [dark gray] curve in Fig. 2), we find that (for all binding PECs used) the simulated KER distribution cannot reproduce the very low experimental KERs. Due to this we will only present the simulated spectra obtained by using the repulsive $f\,^4\Pi_g$ PEC taken from Ref. [10] in the following. The laser parameters are equal for all simulations throughout this work and match the parameters in our experiment: we use an IR-photon energy of 1.65 eV, a pulse length (intensity FWHM) of 12 fs, and a peak intensity of $3 \times 10^{12}\,\mathrm{W/cm^2}$. The dipole coupling matrix elements between the two ionic states are taken from Ref. [8].

A. Simulated spectra based on the $a\,^4\Pi_u$ potential calculated by Magrakvelidze *et al.* [8]

When the quantum simulation is performed with the $a\,^4\Pi_u$ state calculated in Ref. [8] (red [dark gray] curve in Fig. 2) and the repulsive state calculated in Ref. [10] (solid green [light gray] curve in Fig. 2), the obtained KER spectrum is shifted by 50 meV towards lower KERs compared to the experimental data. By treating the position of the $f\,^4\Pi_g$ PEC as a free parameter, we found that shifting it by 0.08 a.u. towards larger internuclear distances (dashed green curve in Fig. 2) is necessary in order to reproduce the experimental KER distribution.

The result of the simulation with the shifted $f\,^4\Pi_g$ PEC is plotted in Fig. 6 (a). A projection of the lower KER band (KER < 0.08 eV) in Fig. 6 (a) is plotted in Fig. 6 (b). The revival time is ≈ 1750 fs. It thus occurs 500 fs later than in our experiment. The QB spectrum corresponding to the simulated time-domain spectrum is shown in Fig. 7 (a). The position of the experimentally observed QB signals is indicated by white boxes. The agreement between theory and experiment is very good near the dominant QB energies ($E_{\mathrm{QB}} \approx 0.1\,\mathrm{eV}$).

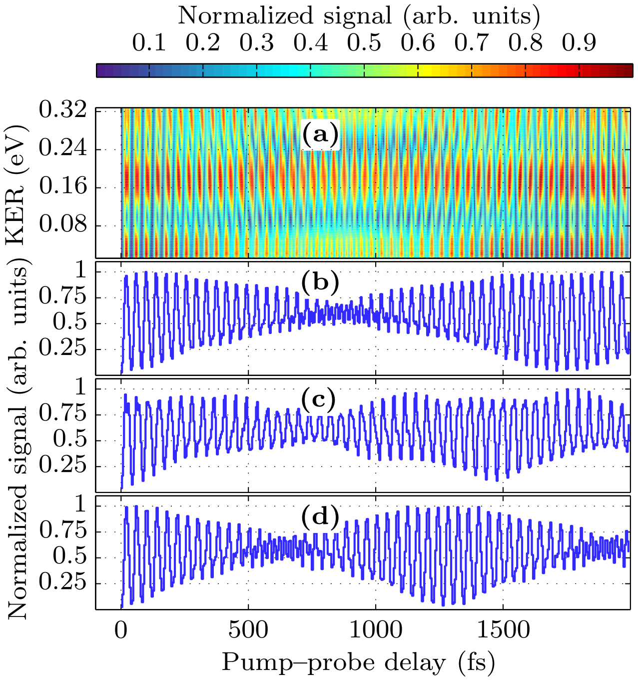

Figure 6. Simulated yield of O^+ fragments as a function of pump–probe delay obtained with a coupled-channel simulation involving different sets of PECs: **(a)** Yield as function of pump–probe delay and KER using the binding $O_2^+(a\,^4\Pi_u)$ potential from Ref. [8] (red [dark gray] curve in Fig. 2) and the repulsive $O_2^+(f\,^4\Pi_g)$ PEC adapted from Ref. [10] (green [light gray] dashed curve in Fig. 2). **(b)** Projection of the lower KER band in (a) onto the time-delay axis. **(c)** Same as (b) but for the binding $a\,^4\Pi_u$ and the repulsive $f\,^4\Pi_g$ PECs from Ref. [10] (green [light gray] solid curves in Fig. 2). **(d)** Same as (b) but using a Morse potential (blue dash-dotted curve curve in Fig. 2) and the repulsive $f\,^4\Pi_g$ PEC adapted from Ref. [10] (green [light gray] dashed curve in Fig. 2).

If instead of the repulsive $f\,^4\Pi_g$ state from Ref. [10] the one calculated in Ref. [8] is used (red [dark gray] curve in Fig. 2), the smallest KERs are larger than 0.1 eV and significantly higher than the smallest KERs observed in the experiment. This minimal KER is due to a small hump in the repulsive PEC at an internuclear distance of 4.5 a.u..

B. Simulated spectra based on the $a\,^4\Pi_u$ and $f\,^4\Pi_g$ potentials calculated by Marian *et al.* [10]

Next, the coupled-channel simulation is performed using the $a\,^4\Pi_u$ and $f\,^4\Pi_g$ states calculated in Ref. [10] (solid green [light gray] curves in Fig. 2). As in the previous case, the simulated O^+ yield as a function of the pump–probe delay and KER is obtained (not shown). The projection of the resulting lower KER band is shown

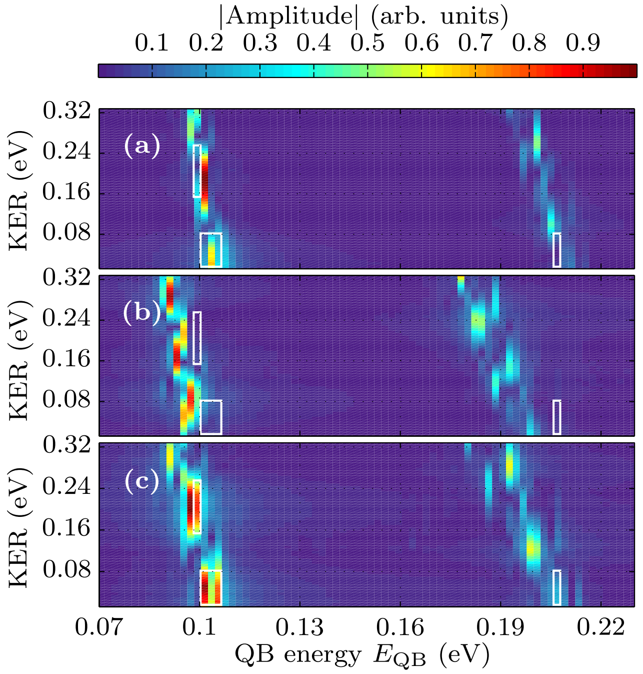

Figure 7. QB spectra of the simulated O^+ yield as function of KER. **(a)** Obtained by using the binding $O_2^+(a\,{}^4\Pi_u)$ potential from Ref. [8] (red [dark gray] curve in Fig. 2) and the repulsive $O_2^+(f\,{}^4\Pi_g)$ PEC adapted from Ref. [10] (green [light gray] dashed curve in Fig. 2). **(b)** Obtained by using the binding $a\,{}^4\Pi_u$ and the repulsive $f\,{}^4\Pi_g$ PECs from Ref. [10] (green [light gray] solid curves in Fig. 2). **(c)** Obtained by using a Morse potential (blue dash-dotted curve curve in Fig. 2) and the repulsive $f\,{}^4\Pi_g$ PEC adapted from Ref. [10] (green [light gray] dashed curve in Fig. 2).

in Fig. 6 (c). The broad revival structure is close to 1500 fs and thus slightly larger than the experimental value of 1270 fs. The QB spectrum corresponding to the delay-dependent spectrum is shown in Fig. 7 (b). We emphasize that for this combination of PECs the agreement with the experimental KER is better if the original $f\,{}^4\Pi_g$ PEC is used instead of the one shifted by 0.08 a.u.. The QB energies are considerably smaller than the ones obtained in experiment. As for the previously discussed case, by using the repulsive curve from Ref. [8] (red [dark gray] curve in Fig. 2) we were not able to reproduce the very low KERs observed in the experiment.

C. Using a Morse potential adjusted to the experimental data

With regard to the repulsive $f\,{}^4\Pi_g$ PEC which has a strong effect on the simulated KER distribution, the comparison with the experimental data seems to favor the PEC calculated in Ref. [10] as very low KERs observed experimentally cannot be reproduced by our simulations using the $f\,{}^4\Pi_g$ PEC from Ref. [8]. As expected, the binding PEC mostly influences the observed QB oscillation and revival time. Even though the revival time obtained with the PEC from Ref. [10] seems to fit slightly better to the experimental data, the QB energy obtained with the PEC from Ref. [8] (especially for the lower KER band at KER $\lesssim 0.08$ eV) is in excellent agreement with the experiment.

In order to demonstrate the sensitivity of the wave-packet dynamics to the exact shape of the binding potential, we additionally propagate a vibrational wave packet within a Morse potential

$$V(R) = D_e\left(e^{-2a(R-R_0)} - 2e^{-a(R-R_0)}\right).$$

The analytical solution for the wave-packet dynamics in the Morse potential, shows that both the width a and the depth D_e determine the QB frequency as well as the revival time [21]. Vice versa, the experimentally observed oscillation period and revival time can be used to deduce the parameters $a = 1.320$ a.u. and $D_e = 0.1007$ a.u.. The potential minimum R_0 remains a free parameter. Here we use the value of $R_0 = 2.61$ a.u. that was determined in a previous experiment [22]. The Morse potential with the described parameters is presented in Fig. 2 (blue dash-dotted curve).

Figure 6 (d) shows the projection of the lower KER band resulting from the coupled-channel simulation using the Morse potential. Even though it deviates only slightly from the theoretically predicted PECs (see Fig. 2), the position and shape of the simulated revival time is in better agreement with the experimental data than for the curves discussed in subsections IV A and IV B above. This is expected since the Morse potential was adjusted to the experimental observables, but nevertheless demonstrates the extreme sensitivity of the wave-packet dynamics on the vibrational level spacing and, therefore, on the shape of the PEC.

The simulated QB spectrum using the Morse potential is shown in Fig. 7 (c). Similar to those with the first pair of PECs [discussed in subsection IV A and shown in Fig. 7 (a)], the repulsive curve calculated in Ref. [10] is shifted by 0.08 a.u. towards larger internuclear distances (plotted as dashed green [light gray] curve in Fig. 2) in order to obtain a KER spectrum that is compatible with the experiment [Fig. 5 (a)]. The broad line at $E_{\mathrm{QB}} \approx 0.1$ eV features two maxima at 0.102 and 0.106 eV, which correspond to the expected vibrational level spacings in the coupling region. In addition, the KER distributions of these lines fit well to the experiment. Only the KER distribution of the events contributing to the signal at $E_{\mathrm{QB}} \approx 0.2$ eV, which is created by a beating between vibrational states with $\triangle v = 2$, is shifted compared to the experimental data: In the simulated spectrum [Fig. 7 (c)] the strongest signal appears at KER ≈ 0.13 eV – in between the KERs featured by the signal at $E_{\mathrm{QB}} \approx 0.1$ eV. In the experimental spectra, however, the KER distribution at $E_{\mathrm{QB}} \approx 0.2$ eV shows only very low KERs, similar to the strong signal at $E_{\mathrm{QB}} \approx 0.1$ eV. The reason for this is currently unknown.

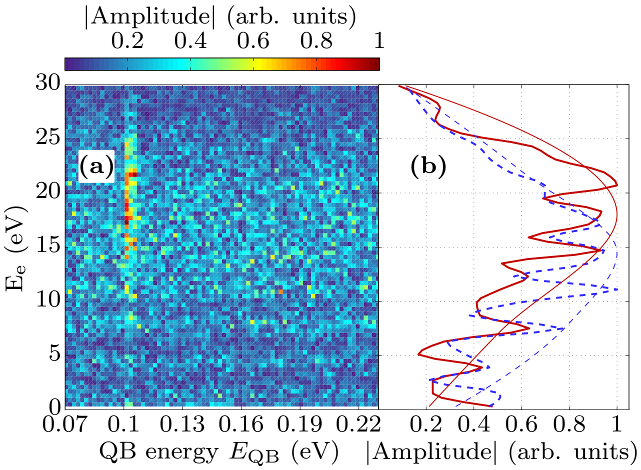

Figure 8. (Color online) **(a)** QB spectrum of photoelectrons measured in coincidence with low energetic O^+. Plotted is the Fourier amplitude as a function of the QB energy and the photoelectron kinetic energy E_e. **(b)** Red bold curve: Projection of the QB signal at $E_{\mathrm{QB}} \approx 0.1\,\mathrm{eV}$ shown in Fig. 8 (a) onto E_e axis. Blue bold dashed curve: Projection of the DC component at $E_{\mathrm{QB}} < 0.005\,\mathrm{eV}$ onto the E_e axis. For better comparison the curves in Fig. 8 (b) the curves are smoothed and normalized. In addition schematic envelopes of the spectra are shown (thin red solid and blue dashed curve).

V. PHOTOELECTRONS

The QB spectrum of the photoelectrons detected in coincidence with O^+ ions of a kinetic energy between 0.013 eV and 0.08 eV – the KER region in which the oscillation is most pronounced – is plotted in Fig. 8 (a). This spectrum is used in the following to further confirm that the PECs involved in the nuclear motion have been identified correctly (compare Refs. [23, 24] for a similar approach). As in the ion spectra, a clear signal is visible at $E_{\mathrm{QB}} \approx 0.1\,\mathrm{eV}$. The red bold curve in Fig. 8 (b) shows a projection of events belonging to this signal onto the E_e axis. The resulting electron spectrum therefore corresponds to photoelectrons created by ionization to the $O_2^+(a\,{}^4\Pi_u)$ state. Additionally, the time-delay independent spectrum is shown in Fig. 8 (b) (blue bold dashed curve). This signal is given by the projection of the DC component, i.e. the signal at $E_{\mathrm{QB}} < 0.005\,\mathrm{eV}$, onto the E_e axis. In the following paragraph we will first discuss the origin of this time-independent spectrum. Afterwards we will discuss why the envelope of the time-dependent spectrum [red thin curve in Fig. 8 (b)] is shifted towards higher E_e compared to the envelope of the background signal [blue thin dashed curve in Fig. 8 (b)].

The peaks in the time-delay independent signal [blue bold dashed curve in Fig. 8 (b)] are separated by ≈ 3.2 eV which is the odd-harmonic spacing of the XUV spectrum ($\triangle E_{\mathrm{HHG}} = 2h\nu_{\mathrm{IR}}$). The fact that the harmonic spectrum is clearly imprinted onto the electron energies is an indication that all significantly contributing PECs feature the same dissociation limit E_1^{diss}, since the electron energy is given by

$$E_e = h\nu_{\mathrm{XUV}} - \mathrm{KER} - E_1^{\mathrm{diss}} \tag{1}$$

and the KER is limited to a small range of energies. As mentioned earlier, the low-energetic, time-delay independent ion yield is expected to be caused by the predissociation out of the $O_2^+(B\,{}^2\Sigma_g^-)$ state (red dash-dotted line in Fig. 1). We therefore assume that the time-delay independent electron spectrum [blue bold dashed curve Fig. 8 (b)] results from the ionization to this state [17]. This state predissociates into the $\mathrm{O}(^1\mathrm{D}) + \mathrm{O}^+(^4\mathrm{S}^0)$ continuum and the dissociation energy is given by $E_1^{\mathrm{diss}} = 20.7\,\mathrm{eV}$.

The time-dependent spectrum [red bold curve in Fig. 8 (b)] results from the ionization to the $a\,{}^4\Pi_u$ PEC and subsequent absorption of an additional IR photon. In this reaction, the molecule dissociates to the $\mathrm{O}(^1\mathrm{D}) + \mathrm{O}^+(^4\mathrm{S}^0)$ continuum with $E_2^{\mathrm{diss}} = 18.7\,\mathrm{eV}$ and the electron energy is given by

$$E_e = h\nu_{\mathrm{XUV}} - \mathrm{KER} - E_2^{\mathrm{diss}} + h\nu_{\mathrm{IR}}. \tag{2}$$

As before, the range of KERs is small. Comparing Eq. 1 and 2, a relative shift of the envelopes of the photoelectron spectra [Fig. 8 (b)] by

$$E_1^{\mathrm{diss}} - (E_2^{\mathrm{diss}} - h\nu_{\mathrm{IR}}) \approx 3.7\,\mathrm{eV}$$

is expected. The predicted shift is in qualitative agreement with the envelopes in Fig. 8 (b). This is a further indication that the PECs involved in the wave-packet dynamics have been identified correctly. The above argument is only valid because the photo-ionization cross sections to the $B\,{}^2\Sigma_g^-$ and the $a\,{}^4\Pi_u$ states are calculated to be more or less constant for a photon energy between 30 and 40 eV [16].

Additionally the electron spectrum can be used to exclude a second reaction pathway, namely

$$\mathrm{O}_2 \xrightarrow{\mathrm{XUV}} \mathrm{O}_2^* \xrightarrow{\mathrm{IR}} \mathrm{O}^+ + \mathrm{O} + \mathrm{e}^-.$$

Here the XUV pulse resonantly excites the molecule and the wave packet oscillates in a PEC of a neutral state. This process cannot be excluded experimentally if only ion spectra are considered. In this case strong-field ionization would take place in the probe step and a low energetic electron would be emitted. The electron-energy spectrum plotted as red curve in Fig. 8 (b), however, excludes this process for two reasons: first the electron yield increases with increasing E_e. In addition the maxima in the electron yield are separated by ≈ 3.2 eV. Both features are signatures of ionization by a single, highly energetic photon created by HHG.

VI. SUMMARY AND OUTLOOK

We performed an XUV–IR pump–probe experiment examining the bound wave-packet dynamics in molecular oxygen ions. With a large pump–probe delay range we are able to fully resolve the first (half-)revival of the wave packet. By Fourier transforming the time-dependent signal, we obtain QB frequencies which are in excellent agreement with the vibrational level spacing of the bound ionic $O_2^+(a\,^4\Pi_u)$ state calculated in Ref. [8].

A previous IR–IR pump–probe experiment [7] reported a beating between six vibrational states, while we only observe a beating between four states. This is probably due to the much higher probe intensity (up to $3\times10^{14}\,\mathrm{W/cm^2}$) used in Ref. [7]. Another important difference between our experimental results and those presented in Ref. [7] is the QB energy resulting from a beating between neighboring vibrational states. It was previously observed at 0.124 to 0.144 eV while we find QB energies between 0.098 and 0.106 eV.

By comparing with coupled-channel simulations different combinations of calculated PECs were tested. While for the repulsive $O_2^+(f\,^4\Pi_g)$ curve, our experimental data favors one of the calculated PECs, neither of the theoretically predicted bound $a\,^4\Pi_u$ states is in full agreement with the experimental spectra. For both PECs either the QB energy or the revival time deviates from the experimental one.

In order to demonstrate the sensitivity of our method to the shape of the binding PEC, we used an adjusted Morse potential in our calculations such that the experimentally observed features are reproduced best. The optimized Morse potential deviates only slightly from the calculated PECs.

Surprisingly, in our experimental data the oscillation amplitude in the revival is stronger than close to the temporal overlap of the pump and probe pulses. A simple explanation for this observation might be a different orientation of the molecule in the pump and the probe step. This hypothesis could be tested in a future experiment by using crossed polarizations in pump and probe pulse.

In principle, our XUV–IR pump–probe scheme can be used to investigate the wave-packet dynamics within any electronic state in a diatomic molecule, as long as this state can be coupled resonantly to a repulsive state by the infrared probe pulse. This has been reported for H_2^+ in Ref [4]. If the probe photon energy could be tuned many additional systems would fulfill this condition. In the case of O_2^+ more vibrational states in the binding potential of the $a\,^4\Pi_u$ state could be accessed by tuning the wavelength of the probe pulse leading to a very detailed probing of the PEC shapes [25, 26].

ACKNOWLEDGMENTS

The authors would like to thank Maia Magrakvelidze for fruitful discussions. TM is grateful for the financial support of JSPS Fellowship for Research Abroad. UT acknowledges partial support by the Chemical Sciences, Geosciences, and Biosciences Division, Office of Basic Energy Sciences, Office of Science, U.S. DOE, the U.S. NSF, and the Alexander von Humboldt foundation.

[1] F. Légaré, K. F. Lee, I. V. Litvinyuk, P. W. Dooley, A. D. Bandrauk, D. M. Villeneuve, and P. B. Corkum, Phys. Rev. A **72**, 052717 (2005).

[2] A. S. Alnaser, B. Ulrich, X. M. Tong, I. V. Litvinyuk, C. M. Maharjan, P. Ranitovic, T. Osipov, R. Ali, S. Ghimire, Z. Chang, C. D. Lin, and C. L. Cocke, Phys. Rev. A **72**, 030702 (2005).

[3] H. Niikura, D. M. Villeneuve, and P. B. Corkum, Phys. Rev. A **73**, 021402 (2006).

[4] F. Kelkensberg, C. Lefebvre, W. Siu, O. Ghafur, T. T. Nguyen-Dang, O. Atabek, A. Keller, V. Serov, P. Johnsson, M. Swoboda, T. Remetter, A. L'Huillier, S. Zherebtsov, G. Sansone, E. Benedetti, F. Ferrari, M. Nisoli, F. Lépine, M. F. Kling, and M. J. J. Vrakking, Phys. Rev. Lett. **103**, 123005 (2009).

[5] F. He and U. Thumm, Phys. Rev. A **81**, 053413 (2010).

[6] S. De, I. A. Bocharova, M. Magrakvelidze, D. Ray, W. Cao, B. Bergues, U. Thumm, M. F. Kling, I. V. Litvinyuk, and C. L. Cocke, Phys. Rev. A **82**, 013408 (2010).

[7] S. De, M. Magrakvelidze, I. A. Bocharova, D. Ray, W. Cao, I. Znakovskaya, H. Li, Z. Wang, G. Laurent, U. Thumm, M. F. Kling, I. V. Litvinyuk, I. Ben-Itzhak, and C. L. Cocke, Phys. Rev. A **84**, 043410 (2011).

[8] M. Magrakvelidze, C. M. Aikens, and U. Thumm, Phys. Rev. A **86**, 023402 (2012).

[9] I. A. Bocharova, A. S. Alnaser, U. Thumm, T. Niederhausen, D. Ray, C. L. Cocke, and I. V. Litvinyuk, Phys. Rev. A **83**, 013417 (2011).

[10] C. M. Marian, R. Marian, S. D. Peyerimhoff, B. A. Hess, R. J. Buenker, and G. Seger, *Molecular Physics*, Mol. Phys. **46**, 779 (1982).

[11] M. Magrakvelidze, O. Herrwerth, Y. H. Jiang, A. Rudenko, M. Kurka, L. Foucar, K. U. Kühnel, M. Kübel, N. G. Johnson, C. D. Schröter, S. Düsterer, R. Treusch, M. Lezius, I. Ben-Itzhak, R. Moshammer, J. Ullrich, M. F. Kling, and U. Thumm, Phys. Rev. A **86**, 013415 (2012).

[12] P. Agostini and L. F. DiMauro, Rep. Prog. Phys. **67**, 813 (2004).

[13] J. Ullrich, R. Moshammer, A. Dorn, R. Dörner, L. P. H. Schmidt, and H. Schmidt-Böcking, Rep. Prog. Phys. **66**, 1463 (2003).

[14] L. Bytautas, N. Matsunaga, and K. Ruedenberg, J. Chem. Phys. **132**, (2010).

[15] B. Feuerstein, T. Ergler, A. Rudenko, K. Zrost, C. D. Schröter, R. Moshammer, J. Ullrich, T. Niederhausen, and U. Thumm, Phys. Rev. Lett. **99**, 153002 (2007).

[16] P. Lin and R. R. Lucchese, J. Chem. Phys. **116**, 8863 (2002).

[17] T. Akahori, Y. Morioka, M. Watanabe, T. Hayaishi, K. Ito, and M. Nakamura, J. Phys. B **18**, 2219 (1985).

[18] J. A. Samson, J. Gardner, and G. Haddad, JESRP **12**, 281 (1977).

[19] T. Gustafsson, Chem. Phys. Lett. **75**, 505 (1980).

[20] C. Lefebvre, T. T. Nguyen-Dang, F. Dion, M. J. J. Vrakking, V. N. Serov, and O. Atabek, Phys. Rev. A **88**, 053416 (2013).

[21] R. Robinett, Physics Reports **392**, 1 (2004).

[22] K. P. Huber and G. Herzberg, *Molecular Spectra and Molecular Structure, Vol. 4* (Van Nostrand Reinold Company, 1979).

[23] E. Gagnon, P. Ranitovic, X.-M. Tong, C. L. Cocke, M. M. Murnane, H. C. Kapteyn, and A. S. Sandhu, Science **317**, 1374 (2007).

[24] W. Cao, S. De, K. P. Singh, S. Chen, M. S. Schöffler, A. S. Alnaser, I. A. Bocharova, G. Laurent, D. Ray, S. Zherebtsov, M. F. Kling, I. Ben-Itzhak, I. V. Litvinyuk, A. Belkacem, T. Osipov, T. Rescigno, and C. L. Cocke, Phys. Rev. A **82**, 043410 (2010).

[25] U. Thumm, T. Niederhausen, and B. Feuerstein, Phys. Rev. A **77**, 063401 (2008).

[26] M. Magrakvelidze, A. Kramer, K. Bartschat, and U. Thumm, J. Phys. B **47**, 124003 (2014).